Environmental Science & Technology

Article

pubs.acs.org/est

Modeling Nanosilver Transformations in Freshwater Sediments

Amy L. Dale,[†,‡] Gregory V. Lowry,[†,§] and Elizabeth A. Casman[†,‡,*]

[†]Center for Environmental Implications of NanoTechnology (CEINT)

[‡]Engineering and Public Policy, Carnegie Mellon University, Pittsburgh, Pennsylvania 15213, United States

[§]Civil and Environmental Engineering, Carnegie Mellon University, Pittsburgh, Pennsylvania 15213, United States

Supporting Information

ABSTRACT: Silver nanoparticles (AgNPs), an effective antibacterial agent, are a significant and fast-growing application of nanotechnology in consumer goods. The toxicity of AgNPs released to surface waters during the use or disposal of AgNP-containing products will depend on the chemical transformations the nanoparticles undergo in the environment. We present a simple one-dimensional diagenetic model for predicting AgNP distribution and silver speciation in freshwater sediments. The model is calibrated to data collected from AgNP-dosed large-scale freshwater wetland mesocosms. The model predicts that AgNP sulfidation will retard nanoparticle oxidation and ion release. The resultant Ag_2S-coated AgNPs are expected to persist and accumulate in sediment downstream from sources of AgNPs. Silver speciation and persistence in the sediment depend on the seasonally variable availability of organic carbon and dissolved oxygen. The half-life of typical sulfidized (85% Ag_2S) AgNPs may vary from less than 10 years to over a century depending on redox conditions. No significant difference in silver speciation and distribution is observed between ≥50% Ag_2S and 100% Ag_2S AgNPs. Formation and efflux of toxic silver ion is reduced in eutrophic systems and maximized in oligotrophic systems.

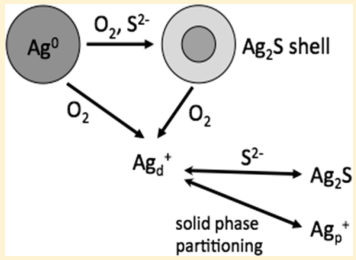

INTRODUCTION

The global market for nanotechnology is estimated to have reached $16 billion in 2010 and is expected to grow to approximately $27 billion by 2015.[1] Products containing silver nanoparticles (AgNPs), such as antibacterial cosmetics and textiles, represent a major use of nanotechnology in the consumer goods sector.[2] AgNPs are toxic to a wide range of organisms,[3] and textiles and cosmetics demonstrate relatively high environmental releases;[4] initial estimates suggest AgNP emissions to air, soil, and water during manufacturing, use, disposal, and/or recycling may equal as much as 50% of annual production.[5]

The toxic effects of as-manufactured, untransformed silver nanoparticles, which are mostly Ag^0, have been observed in microorganisms, algae, fungi, vertebrates, invertebrates, and aquatic and terrestrial plants.[3] AgNPs tend to oxidize in oxic aquatic environments.[7−11] This process releases silver ions (Ag^+), which can nonselectively interfere with cell respiration and membrane transport.[3] The toxic effects of silver are exacerbated by the tendency of the ionic form to persist and bioaccumulate.[12,13]

Another particulate species, silver sulfide (Ag_2S), forms in the presence of naturally occurring sulfides. In an oxygen-mediated process termed "sulfidation," the AgNPs react with sulfide to form a surface layer of Ag_2S.[14] Partial sulfidation results in what has been termed a core−shell structure, although TEM images have shown that complex Ag^0-Ag_2S morphologies may also occur.[3,7,14] Complete sulfidation is possible.[14] In 2010, Kim et al. characterized Ag_2S NPs found in sewage sludge and proposed that that the sulfide-rich, anoxic environment of sewage treatment plants (STPs) facilitates rapid sulfidation.[15] This transformation is of great importance, both because the highly insoluble Ag_2S shell reduces the rate of AgNP oxidation[7] and because Ag_2S is less toxic to microorganisms than Ag^0 NPs and Ag^+.[3,16,17]

The differential toxicity of silver species necessitates the development of environmental fate models that can predict their relative abundance in a system of interest. Although several models have recently been developed to describe nanoparticle transport in environmental media,[18−23] no attempts have been made to model the complex chemical transformations of AgNPs in surface waters or sediments.

Smoluchowski coagulation theory indicates nanoparticles will heteroaggregate rapidly with clays, minerals, and other natural colloids upon entering surface water.[24] Aggregation is expected to lead to settling, which will lead in turn to accumulation of NPs in sediments.[24−26] This conclusion is borne out by laboratory experiments on the behavior of nanoparticles,[27,28] as well as the most recent mathematical models of nanoparticle fate and transport in surface waters.[18,21−23]

The biodiversity and health of aquatic systems can be negatively impacted by the biouptake of AgNPs and toxic Ag^+ by sediment-dwelling organisms. Biomagnification resulting from ingestion of sediment-dwelling organisms by species higher in the food web is a potential concern,[29] since trophic transfer of

Received: May 27, 2013
Revised: October 20, 2013
Accepted: October 22, 2013
Published: October 22, 2013

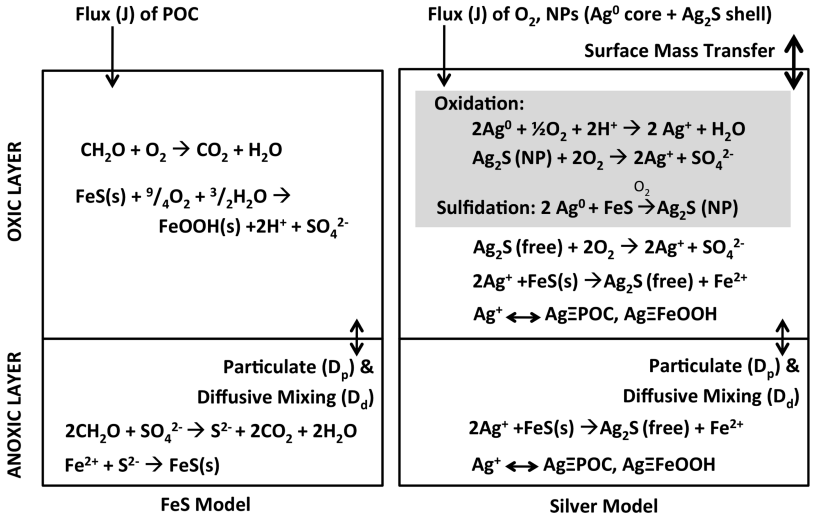

Figure 1. Model schematic for nanosilver sediment chemistry (adapted from ref 31). Nanoparticle reactions are highlighted in gray and represent an extension of the model proposed by Di Toro et al. (1996) for cadmium speciation and solid phase partitioning.

NPs has been reported in a simulated terrestrial ecosystem.[30] Resuspension of particulate silver species and diffusion of silver ion from sediments are also possible sources of silver in the water column.

The model developed in this paper is based on a mass balance model by Di Toro et al.[31] that describes the speciation of cadmium in sediments in response to redox conditions established in the sediment as a function of oxygen consumption during organic carbon diagenesis, or mineralization.[32,33] As described below, this adaptation is appropriate because the speciation of both Ag and Cd in sediments is contingent on the displacement of iron from iron sulfide to form highly stable (i.e., very low solubility) metal sulfides.[34] The model was calibrated to experimental data collected from Ag^0 NP-dosed artificial freshwater wetland mesocosms operated by the Center for Environmental Implications of Nanotechnology (CEINT). The reader is referred to Lowry et al. (2012) for an in-depth treatment of the mesocosm experiment.[35] After calibration, several input scenarios were selected for further investigation.

MATERIALS AND METHODS

Model Structure and Framework. Figure 1 outlines the reactions and physical processes modeled. The diagram distinguishes between oxic and anoxic sediment layers for visual simplicity; however, concentrations of oxygen and all other species were modeled continuously over depth.

Silver ion, Ag^+, is derived from the oxidation of the elemental silver (Ag^0) core of the AgNPs or from the oxidation of sulfur in silver sulfide. Silver sulfide exists either as a coating on the particle surface, Ag_2S (NP), or as a free (not bound to the initial AgNP) inorganic precipitate formed by the interaction of iron sulfide with silver ion diffusing freely in the pore water, Ag_2S (free). This distinction between the two locations of Ag_2S, "NP" and "free," was necessary to properly track the extent of sulfidation of the AgNPs during the simulation. This approach distinguishes transformations undergone by the nanoparticles from those undergone by the silver ions released from the particles. No such distinction was necessary for Ag^0, which is assumed to be present only in the AgNP cores. The relevant reactions are as follows:

$$2Ag^0 + 1/2O_2 + 2H^+ \rightarrow 2Ag^+ + H_2O \quad (1)$$

$$Ag_2S(NP) + 2O_2 \rightarrow 2Ag^+ + SO_4^{2-} \quad (2)$$

$$Ag_2S(free) + 2O_2 \rightarrow 2Ag^+ + SO_4^{2-} \quad (3)$$

The main driver of aerobic AgNP oxidation is the depth of oxygen penetration in the sediments, which depends primarily on its consumption during the microbially mediated oxidation of particulate organic carbon (POC):

$$CH_2O + O_2 \rightarrow CO_2 + H_2O \quad (4)$$

Silver ion freely diffusing in the pore water is converted to silver sulfide, Ag_2S (free), via a displacement reaction, in which iron sulfide acts as the source of sulfide.

$$2Ag^+ + FeS(s) \rightarrow Ag_2S(free) + Fe^{2+} \quad (5)$$

Iron sulfide serves as a proxy in the model for all available sulfides in the system (e.g., acid-volatile sulfide, or AVS). Iron sulfide is gained via the anaerobic oxidation of organic carbon, which reduces sulfate to sulfide,

$$2CH_2O + SO_4^{2-} \rightarrow S^{2-} + 2CO_2 + 2H_2O \quad (6)$$

$$Fe^{2+} + S^{2+} \rightarrow FeS(s) \quad (7)$$

and is lost by oxidation to form iron oxyhydroxide (FeOOH):

$$FeS(s) + 9/4O_2 + 3/2H_2O \rightarrow FeOOH(s) + 2H^+ + SO_4^{2-} \quad (8)$$

Finally, iron oxyhydroxide and particulate organic carbon reversibly sorb silver ion.

$$Ag^+ \leftrightarrow Ag \equiv POC \quad (9)$$

$$Ag^+ \leftrightarrow Ag \equiv FeOOH \quad (10)$$

Physical processes modeled include particle mixing due to bioturbation, diffusive mixing of dissolved species, efflux of dissolved species as a result of diffusion at the sediment-water interface, and influx of organic carbon, AgNPs, and oxygen. Note that, in the tradition of conventional mass balance models, "particle" refers here to all particulate (solid phase) species: POC, FeS, FeOOH, Ag^0, Ag_2S ("NP" and "free"), Ag≡POC, and Ag≡FeOOH. "Nanoparticle" refers only to the particulate

Table 1. Ranges of Model Parameters[a,b]

symbol	parameter	units	value
ϕ_0	sediment porosity at the sediment-water interface[40]	m^3/m^3-bulk	(0.25, 0.4, **0.99**)
k^{ϕ}	rate of decrease in sediment porosity with depth	m^{-1}	***0.058***
ρ	sediment density[33]	g-sed/m^3-sed	(1.5×10^6, $\mathbf{2.5 \times 10^6}$, 2.7×10^6)
D_d	diffusive mixing coefficient[33]	m^2/d	(7.0×10^{-5},$\mathbf{7.5 \times 10^{-5}}$, 1.7×10^{-4})
D_p	particle mixing coefficient[41]	m^2/d	(5.5×10^{-11}, $\boldsymbol{4.0 \times 10^{-7}}$, 1×10^{-4})
z_{D_p}	e-folding depth of particle mixing[41]	m	(0.02, **0.10**, 0.30)
f_{POC_1}	fraction of POC in G_1 reactivity class[33]	[−]	0.50-**0.65**
f_{POC_2}	fraction of POC in G_2 reactivity class[33]	[−]	0.16-**0.25**
k_{POC_1,O_2}	rate of aerobic oxidation of G_1 carbon[33]	d^{-1}	(0.019, **0.048**, 0.07)
k_{POC_2,O_2}	rate of aerobic oxidation of G_2 carbon[33]	d^{-1}	(0.0038, **0.004**, 0.0088)
k_{POC_1,SO_4}	rate of anaerobic oxidation of G_1 carbon[33]	d^{-1}	(0.02, **0.024**, 0.027)
k_{POC_2,SO_4}	rate of anaerobic oxidation of G_2 carbon[33]	d^{-1}	(0.0012, **0.002**, 0.003)
K_{M,O_2}	half saturation constant for POC oxidation using O_2[33]	mg O_2/m^3	**100**
k_{FeS,O_2}	rate of oxidation of FeS to form FeOOH[33]	$d^{-1}(mg\ O_2/m^3)^{-1}$	(3×10^{-6}, **0.001**, 3)
$k_{Ag^0,O_2}((S/Ag)=0)$	rate of Ag^0 NP dissolution[7,9,11]	$d^{-1}(mg\ O_2/m^3)^{-1}$	(1.3×10^{-8}, $\boldsymbol{8.5 \times 10^{-6}}$, 5.1×10^{-4})
k_{sulf}	rate of AgNP sulfidation (long-term average)[14,36]	(mmol S^{2-}/m^3) (mg O_2/m^3)d^{-1}	(0, $\mathbf{2.0 \times 10^{-7}}$, 3.5×10^{-5})
c_{pass}	rate of decrease in k_{Ag^0,O_2}, k_{sulf} as a function of S/Ag[7]	[−]	(14, **20**, 24)
$f_{Ag^0,init}$	fraction Ag^0 by mass in input dose of NPs[6]	[−]	(0, **0.15**, 1.0)
k_{Ag_2S,O_2}	rate of oxidation of sulfur in Ag_2S[42]	$d^{-1}(mg\ O_2/m^3)^{-1}$	(0, $\mathbf{1.5 \times 10^{-7}}$, 4.5×10^{-7})
k_{disp}	rate of displacement reaction[33]	d^{-1}(mmol FeS/m^3)$^{-1}$	**0.1**
$J_{POC,max}$	max annual flux of organic carbon from overlying water[43,44]	mg/m^2-d	(75, **150**, 300)
$\log K_{OC}$	partition coefficient to POC[45]	L/kg	(4.1, **7.3**, 7.8)
σ_{OC}	sorption capacity for POC[33]	μmol/g	$\mathbf{1.7 \times 10^3}$
K_{FeOOH}	partition coefficient to FeOOH[33]	m^3/mmol	$\mathbf{1.0 \times 10^3}$
σ_{FeOOH}	sorption capacity for FeOOH[33]	mol/mol	**0.2**
π_{FeS}	partition coefficient for FeS: $[FeS_p]/[FeS_d]$[33]	m^3/g	$\mathbf{10^{-4}}$-10^{-2}
Initial and Boundary Conditions			
$_{O_2(z=0)}$	oxygen concentration at the interface	mg/m^3	(500, **3600**, 14,000)
$_{foc(t=0)}$	fraction of organic carbon in sediment (at $t = 0$)[33,38]	[−]	(0.001, **0.02**, 0.15)
$_{FeS(t=0)}$	sediment iron sulfide (AVS) concentration (at $t = 0$)[33]	μmol/g	(0.01, **10**, 100)

[a]Nominal values are bolded and values determined by calibration are italicized. Note that nominal values represent a "typical" freshwater system and do not necessarily correspond with the values used to calibrate the model, which were selected to match conditions in the mesocosms. [b]See note in SI Table S3 on the selection of Arrhenius temperature coefficients for mixing and reaction rates (not shown).

species representing the core and shell of the transforming AgNP (Ag^0 and Ag_2S (NP), respectively).

Supporting Information (SI) Table S1 lists the model state variables. Changes in the depth profile of each state variable over time are modeled dynamically using the one-dimensional continuous advective-dispersive mass balance equation:

$$\frac{\partial[C(z)]}{\partial t} - \frac{\partial}{\partial z}\left((f_p D_p(z) + f_d D_d)\frac{\partial[C(z)]}{\partial z}\right) = \sum_j R_j \quad (11)$$

where $C(z)$ is the concentration at depth z, f_p is the particulate fraction of the total concentration, D_p is the particle mixing coefficient, f_d is the dissolved fraction of the total concentration, D_d is the diffusive mixing coefficient, and $\Sigma_j R_j$ represents all reactions resulting in gain or loss of the species.

Reactions. In general, reaction rates were assumed to exhibit a linear dependence on the concentrations of all reactants.[31] The exceptions to the assumption of linear dependence were aerobic and anaerobic oxidation of organic carbon, for which we applied the Michaelis Menton expression for oxygen dependency. SI Table S2 summarizes the reaction equations, which are of the general form

$$R_j = k_j \theta_j^{(T-20)}[C_1][C_2] \quad (12)$$

where k_j is the reaction rate constant, θ_j is the Arrhenius temperature coefficient, T is the temperature in degrees Celsius, and $[C_1]$ and $[C_2]$ are the concentrations of the reactants.

Previous work suggests the rate constants for AgNP oxidation and AgNP sulfidation, k_{Ag^0,O_2} and k_{sulf}, decrease exponentially in response to AgNP sulfidation.[7,14,36] The AgNP oxidation rate was thus modeled using eq 13, where S/Ag represents the molar ratio of sulfur to silver. AgNP sulfidation, in contrast, could not be accurately modeled using eq 13 without drastically reducing the time step (and vastly increasing model runtime). For fully unsulfidized AgNPs, the rate of sulfidation was assumed to decrease rapidly upon dosing so that a constant "long-term average" sulfidation rate would be appropriate over the time scale considered (see SI Table S3 for details). The effect of additional factors (e.g., temperature, pH, organic carbon, particle size, capping agent)[8,10] on the initial rate of AgNP oxidation before sulfidation (S/Ag = 0) was captured by calibration.

$$\mathrm{S/Ag} = \frac{[\mathrm{Ag_2S(NP)}]}{[\mathrm{Ag^0}] + 2[\mathrm{Ag_2S(NP)}]}$$

$$k_{\mathrm{Ag^0,O_2}} = \{k_{\mathrm{Ag^0,O_2}}(\mathrm{S/Ag} = 0)\}e^{c_{\mathrm{pass}}(\mathrm{S/Ag})} \quad (13)$$

Partitioning. For simplicity, all dissolved sulfides were modeled as the dissolved form of FeS using the partitioning coefficient π_{FeS}. The governing equations for iron sulfide "partitioning" are provided by Di Toro et al. (1996). Equilibrium partitioning of silver between the sediment pore water (Ag^+) and the relevant solid phases (Ag≡POC and Ag≡FeOOH) was described with a Langmuir isotherm analogous to that described by Di Toro et al. for cadmium.[31] Details are provided as SI (equations S1−S7). The complexation of Ag with chloride ion, while strong, is significantly less so than for sulfide and for organic matter,[37] and is assumed to be negligible in the freshwater (low chloride) environment. AgCl(s) was not detected by XAS measurements on the mesocoms sediments.[35]

Particle Mixing and Porosity. The particle mixing coefficient, which represents the rate of sediment mixing as a result of biological activity, is temperature-dependent and is assumed to decrease exponentially with depth, z, according to the equation

$$D_\mathrm{p}(z) = D_\mathrm{p}\theta_{D_\mathrm{p}}^{(T-20)}\mathrm{e}^{-z/z_{D_\mathrm{p}}} \quad (14)$$

where $z_{D\mathrm{p}}$ represents the depth of bioturbation.

Since sediments at depth are compacted by the weight of overlying layers, porosity was assumed to decrease exponentially with a decay constant of k^ϕ from a value of 0.99 at the interface (ϕ_0) to a value of 0.25 at depth. Porosity at the interface and at depth was estimated from mesocosm data[35] which produced good agreement between silver concentrations vs depth observed in the mesocosms and those predicted by the model.

Temperature. Annual temperature variation is assumed to be sinusoidal. Coefficients were estimated from water column temperatures in the mesocosms used to calibrate the model[35] and air temperature data at the mesocosm site (http://ceint.duke.edu/chart/mesocosm-air-temp). Higher temperatures increase rates of reaction and solute diffusion via Arrhenius temperature coefficients (not shown in Table 1; see SI Table S3) and correspond with increases in biological activity in the sediment and water column. This leads to higher particle mixing, higher organic carbon influx to the sediment, and the depletion of dissolved oxygen.

Parameter Values. Table 1 summarizes parameter values used in the simulations. SI Table S3 presents the assumptions underlying the selected values. Sensitivity analysis revealed that model outputs were not overly sensitive to local variation in those parameters for which only point estimates were found (SI Table S4).

The nominal values of four model parameters (k^ϕ, D_p, K_{oc}, $k_{\mathrm{Ag^0,O_2}}((\mathrm{S/Ag})=0)$) were determined by calibration. System parameters were matched to conditions in the mesocosms, including loss on ignition (L.O.I. $\approx 2f_{\mathrm{oc}}$,[38] where f_{oc} is the initial organic carbon composition of the sediment), sediment AVS, oxygen concentration at the sediment-water interface, annual temperature variation, AgNP mass input, and time of dosing.[35] The simulation was run for t = 18 months after introducing a simulated pulse input of 2.9 g of "pristine" (unsulfidized) Ag^0 NPs. The AgNPs added to the mesocosms had a thin oxidized Ag (e.g., Ag_2O) shell,[35] which was an implicit determinant of the initial rate of nanoparticle oxidation, $k_{\mathrm{Ag^0,O_2}}((\mathrm{S/Ag})=0)$. For the calibration, mean total silver concentrations calculated by the model over sediment depths of 0−1 cm, 1−2 cm, 2−4 cm, and >4 cm were matched to the median silver concentrations observed in the mesocosms eighteen months after dosing. Model outputs were also matched to the relative abundances of Ag^0, Ag^+-organics, and Ag_2S in the surficial sediments of the mesocosms eighteen months after dosing, as determined from linear combination fits of X-ray absorption spectroscopy (XAS) spectra collected on surficial sediment in the mesocosms.[35] The calibration was performed using the nonlinear parameter estimation software PEST (http://www.pesthomepage.org/), which minimizes the weighted sum of the squared residuals. Weights were calculated as the inverse standard deviation of each field observation.

Silver ion efflux from the sediment to the overlying water at time t was estimated by the model from the predicted concentration profile of Ag^+ at the sediment-water interface.

Solution Method. A fully implicit finite difference approximation was used to simultaneously solve the mass balance equations for all state variables. The Gauss-Seidel iteration method (e.g., as described by Ramaswami et al.[39]) was used to achieve rapid convergence. To avoid dynamic instability associated with the central differencing approach to numerical methods,[39] model resolution (Δz = 1 mm, Δt = 0.05 days) was chosen to ensure

$$\Delta t \le \frac{(\Delta z)^2}{2D_{\max}} \quad (15)$$

where $D_{\max}$ was the maximum value of the time- and depth-dependent diffusion coefficients D_p and D_d.

An exponentially expanding spatial grid was implemented in order to focus computational efforts on transformations occurring near the sediment-water interface while eliminating undue computational burdens at depth (see SI equations S8−S17 for details).[46,47] Model results for the expanded grid were compared to those for an unexpanded grid to affirm the accuracy of the method.

The diagenetic model was run for a year before simulated introduction of the AgNPs to ensure periodicity in seasonally variable redox conditions had been achieved.

Initial and Boundary Conditions. No-flux boundary conditions were assumed at the sediment-water interface for all particulate species except those entering the system—POC, Ag^0, and Ag_2S (NP)—which assumed known influx (Type II/Neumann) boundaries. This boundary condition was assumed to be sufficient to capture the net effect of particle deposition and resuspension in a quiescent wetland environment. Influx of organic carbon was described piecewise in time with a sine curve that peaked at $J_{\mathrm{POC,max}}$ in summer (mid-May to mid-September) and was 15 mg/m^2-d in fall, spring, and winter. This idealized influx scenario agrees with seasonal trends in community respiration and carbon mineralization observed in a freshwater marsh.[48] Known constant concentration (Type I/Dirichlet) boundaries were assumed for all dissolved species. ICP-MS analysis of mesocosm water column samples detected no total silver after initial settling (detection limit of <2 μg/L),[35] so it was assumed that the silver ion concentration at the sediment−water interface could be approximated as zero. At t = 0, the oxygen concentration was decreased linearly from its value at the interface to zero at a depth of 5 mm. The depth profile of oxygen

exhibited exponential decay within one day of launching the simulation.

The mesocosms were dosed with 4.2 g of polydisperse, partially oxidized (80−85 wt % Ag^0) 30−80 nm PVP-coated AgNPs, resulting in initial water column concentrations of 25 mg/L AgNPs. Ag^0 was assumed to exhibit an exponentially declining flux such that all silver added to the water column as a finite square pulse input would penetrate the sediment within 10 days, as observed in the mesocosms.[35] At depth, no-flux boundary conditions were implemented for all species.

RESULTS

Figure 2 compares total Ag concentration vs depth as measured in the mesocosm sediment to the simulated concentration profile

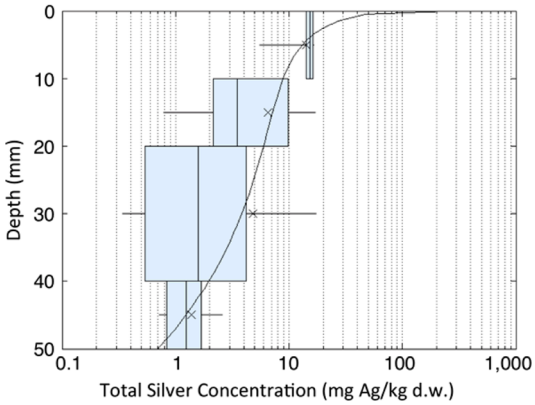

Figure 2. Total sediment silver concentration profile predicted by the model (curve) versus sample data collected from the water-column-dosed mesocosm eighteen months after dosing (boxplots). Boxplots describe the distribution of nine sample measurements (six measurements for the >40 mm depth) at each of four sediment depths (0−10 mm, 10−20 mm, 20−40 mm, >40 mm). Crosses (×) indicate mean values.

of total silver, which represents the sum of all silver species in the system: Ag^0, Ag_2S ("NP" and "free"), Ag^+, Ag≡POC, and Ag≡FeOOH. Silver concentrations (in mg Ag/kg dry weight of sediment) are highest at the sediment-water interface, since the dry weight of sediment in a given volume is lowest when porosity is high. Calibration to XAS data on the speciation of silver in the surficial sediments (~5 mm depth) of the mesocosms 18 months after dosing ensured that, as reported,[35] silver was present as 55% Ag_2S ("NP" and "free", in our model), 27% Ag^+−organic compounds (Ag≡POC), and 18% Ag^0. The concentrations of the other silver species considered in the model (Ag^+, Ag≡FeOOH; see Figure 1) were low (<0.01%).

For those parameters with ranges estimated from the literature ($k_{Ag^0,O_2}((S/Ag)=0)$, D_p, K_{oc}), calibrated values fall within their expected range (italicized values in Table 1). The initial rate of AgNP dissolution, $k_{Ag^0,O_2}((S/Ag)=0)$, exceeds rate constants estimated from the equilibrium solubility of equivalently sized (38−80 nm) AgNPs (3×10^{-8} to 2×10^{-6} $d^{-1}(mg\ O_2/m^3)^{-1}$), assuming 8.6 mg/L DO (as reported) and the reaction rate equation used in the model.[11] The difference may be explained by partial oxidation of the mesocosm AgNPs before dosing (15−20 wt %),[35] which facilitates rapid initial oxidation.[49] In contrast, $k_{Ag^0,O_2}((S/Ag)=0)$ was lower than rates predicted for 40−80 nm AgNPs at pH 4 (8.6 mg/L DO assumed).[9] The AgNP oxidation rate is expected to decrease with an increase in pH.[8]

The calibrated value of the silver ion-organic carbon partitioning coefficient is on the upper end of its expected range (log K_{oc} = 4.1−7.8 L/kg). This suggests the organic carbon in the mesocosms sediments had a relatively high affinity for Ag^+, perhaps due to the presence of strong chelating groups like reduced sulfur. The overall correlation coefficient representing agreement between model output and mesocosm data is 0.997.

Figure 3a shows the silver ion efflux from the sediment to the overlying water as a function of time for a simulated pulse input of 2.9 g of AgNP under typical environmental conditions for a freshwater wetland (the "nominal" case; see bolded values in Table 1). The modeled system was "dosed" in July in order to maximize initial efflux. This represents a worst-case scenario, in which the maximum amount of toxic Ag^+ escapes into the water column before the nanoparticles have the chance to sulfidize and AgNP oxidation rates decrease.

Changes in the depth profile of all state variables over time are provided in SI Figure S2. Oxygen concentration peaks in winter, as has been observed in natural systems.[48,50] However, Ag^+ efflux peaks in summer. SI Figure S3 reveals the mid-July peak in Ag^+ efflux is driven by the temperature dependence of mixing and reaction rates.

The five scenarios in Figure 3 demonstrate the role sulfidation plays in the release of Ag^+ from AgNPs. Scenarios include an unrealistic worst case, in which a pulse input of pristine Ag^0 NPs enters the system (t = 0) and the AgNP sulfidation process is artificially turned off (i.e., nanoparticles remain 100% Ag^0 over the course of the simulation). The other four scenarios demonstrate system responses to a dose of pristine particles (0% Ag_2S before dosing), fully sulfidized particles (100% Ag_2S before dosing), and partially sulfidized particles (50% and 85% Ag_2S before dosing) when sulfidation is allowed to occur. This last scenario (85% Ag_2S) reflects the extent of sulfidation expected for silver particles exiting a sewage treatment plant by way of effluent.[6] Figure 3b shows depth profiles under these four scenarios one year after dosing.

We observe no differences in the extent of AgNP oxidation and the speciation, solid phase partitioning, and efflux of silver ion over time between 50%, 85%, and 100% Ag_2S nanoparticles. This is because the rate of AgNP oxidation decreases exponentially with the extent of AgNP sulfidation (eq 13). AgNPs that enter the system fully unsulfidized similarly behave as if fully sulfidized within a year of dosing, although elevated Ag_2S (free) concentrations are observed as a result of AgNP oxidation—and subsequent reaction of the released Ag^+ with sulfide—within the first several months.

Figure 3b (top right panel) reveals that the predominant form of silver in the sediment will be the partially or fully sulfidized nanoparticles. Percent sulfidation decreases with depth in this pulse input case because the AgNPs that remain at the interface longer spend more time in the presence of O_2. Although FeS and O_2 do not coexist at equilibrium,[14] O_2 mediates AgNP sulfidation. The principal forms resulting from speciation and solid phase partitioning of Ag^+ released during AgNP oxidation are the thermodynamically favored species, Ag_2S (free), and Ag≡POC (silver associated with particulate organic carbon). This is unsurprising, since silver reacts strongly with the sulfur-containing functional groups prevalent in organic compounds. Ag≡POC may be especially high in this model because of the high K_{oc} value determined by calibration. Truly dissolved (highly toxic) Ag^+ is present only at very low concentrations, consistent with observations in field samples.[42]

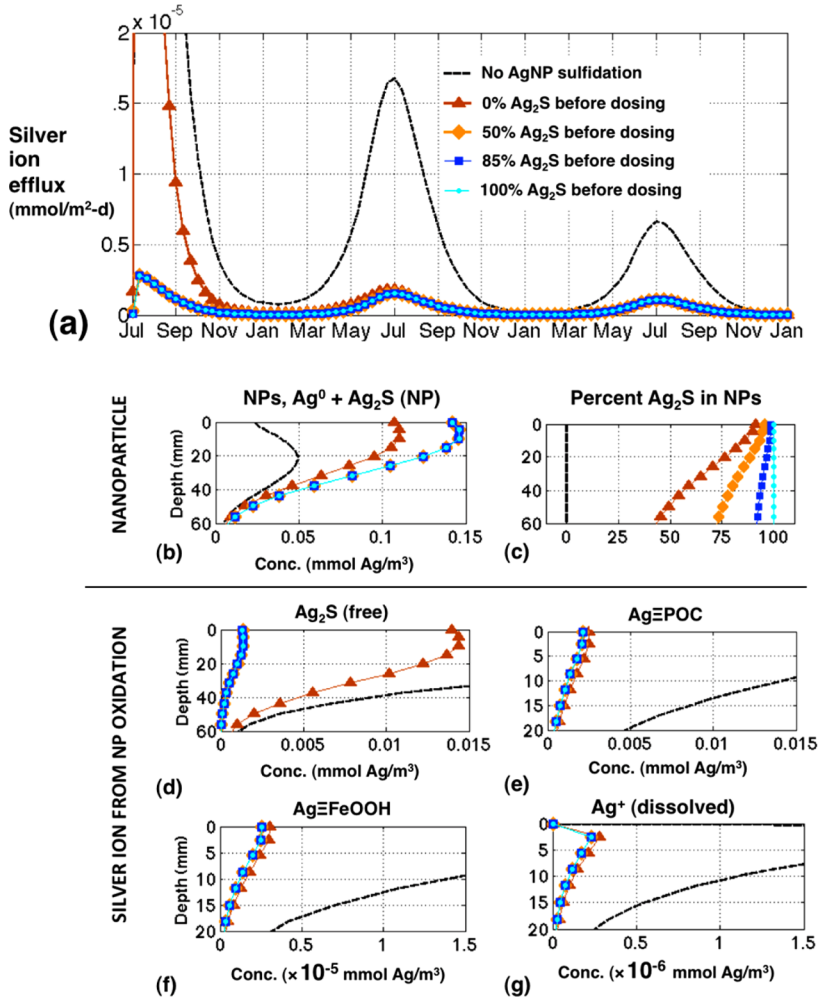

Figure 3. Results for nominal case under five different AgNP percent sulfidation scenarios. (a) Silver ion efflux vs time after dosing, (b) Concentration profiles in the sediment one year after dosing in July. The black dashed curve indicates the unrealistic upper bound on AgNP oxidation, in which the system is dosed with pristine particles (0% Ag_2S) and sulfidation is not allowed to occur. Colored curves correspond with NP inputs that are 0%, 50%, 85%, and 100% sulfidized before dosing when sulfidation is allowed to occur.

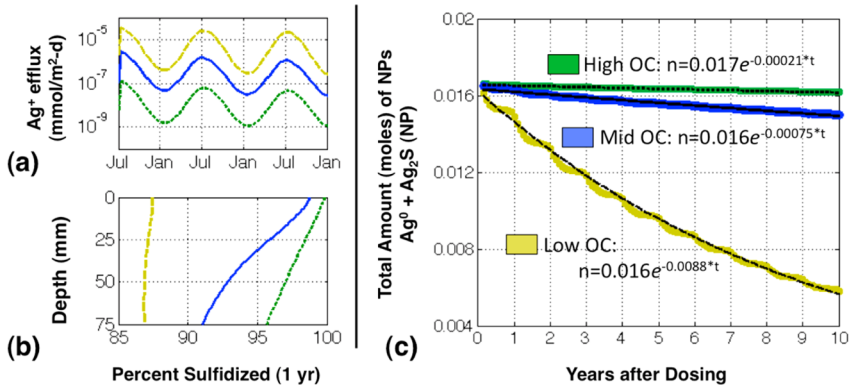

Figure 4. System response to low ($J_{POC,max}$ = 75 mg/m^2-d, f_{oc} = 0.001), mid ($J_{POC,max}$ = 150 mg/m^2-d, f_{oc} = 0.02; the "nominal" case in Figure 3), and high ($J_{POC,max}$ = 300, f_{oc} = 0.15) levels of organic carbon (OC) for 85% sulfidized AgNPs. (a) Ag^+ efflux vs time. The semilog scale reveals orders-of-magnitude differences between the three scenarios. (b) AgNP sulfidation as a function of depth one year after dosing (July). (c) Total amount (moles) of AgNPs in system over time. Nanoparticle half-life time is primarily a function of oxidant availability in the sediment. The decrease in total AgNP amount within 10 years of dosing was fit to an exponential function, where t was expressed as months after dosing. AgNP half-lives estimated from the best-fit curves are 6.6 years (low OC), 77 years (mid OC), and 280 years (high OC).

The normalized sensitivities of model outputs to small (±0.05%) changes in model inputs around the nominal case (i.e., elasticities), reported in SI Table S4, reveal that environmental conditions strongly affect the system response. Figure 4 describes oxidation, sulfidation, and persistence of the AgNPs as a function of organic carbon content.

Aerobic diagenesis of carbon in high organic carbon systems results in low oxygen availability, and subsequent sulfate reduction results in high sulfide availability. Thus Ag^+ efflux occurs less readily (Figure 4, top left panel) but sulfidation occurs more readily (Figure 4, bottom left panel) in high OC systems. The half-life of the 85% sulfidized AgNPs was found to vary from 6.6 years to as much as 280 years in the model depending on oxygen availability (Figure 4, right panel). AgNP half-lives were relatively insensitive to whether the particles were partially sulfidized or pristine (100% Ag^0) upon dosing—half-lives for the pristine AgNPs ranged from 3 months (low OC) to 280 years (high OC). Loss of Ag^0 from the AgNP cores (SI Figure S4) results from Ag^+ formation and sulfidation, and does not exhibit first-order exponential decay.

The mesocosm experiment used a single pulse input of a relatively high concentration of AgNPs. A continuous input of low concentrations of nanoparticles from a wastewater treatment plant is a more realistic scenario. We assumed a continuous input scenario in which 20 million gallons per day of STP effluent (76,000 m^3/d) containing 33 μg/L 85% sulfidized AgNPs were released to a small (75 km^2) lake, and that all silver entered the sediments. Results for the constant input case are provided in SI Figures S5 and S6. Trends agree with those observed in the pulse input case (Figure 4). AgNP accumulation occurs over time in this chronic low dose input case.

DISCUSSION

Nanoparticles are expected to accumulate in sediments after release to surface waters. The toxicity of surface-reactive nanoparticles in environmental media depends greatly on chemical transformations undergone by the nanoparticles and released ions. Recent work has shown particle properties strongly affect AgNP transformations.[9−11] The present work reveals environmental conditions also play an important role.

Particulate organic carbon (POC) diagenesis has long been recognized as a key determinant of oxygen penetration depth and a driving force for sediment processes. The model suggests this process similarly drives AgNP transformations in sediments. Eutrophic (high organic carbon, low oxygen, high AVS) systems maximize rates of AgNP sulfidation and minimize toxic silver ion production and diffusion into the water column. AgNPs may persist in a partially or fully sulfidized form for over a century under these conditions.

Seasonal redox cycles may play a role in silver speciation, bioavailability, and toxicity. The model predicts Ag^+ efflux will be lowest in winter and highest in summer, although seasonal patterns in oxygen availability will vary across natural systems as a function of temperature, organic carbon, light, water currents, and bioturbation.[51] Figure 4 reveals that seasonal variation becomes relatively unimportant over long time scales, especially when compared to the importance of intersite heterogeneity in sediment conditions.

The rate of AgNP oxidation was assumed to decrease exponentially with AgNP sulfidation (eq 13). Because sulfidation occurs readily in the sediments in the nominal case, the initial extent of sulfidation becomes relatively unimportant within a year of dosing (Figure 3). AgNPs that are ≥50% Ag_2S by mass, as expected for AgNPs released to natural waters, will exhibit behavior effectively identical to that of fully sulfidized (100% Ag_2S) NPs.

The AgNP oxidation and sulfidation rates used here are specific to 30 nm AgNPs. They do not account for the inverse relationship between AgNP size and rates of transformation (e.g., as observed by refs 14,16, and 36 and captured by the ranges in Table 1) or the effects of aggregation. In a toxicity study on earthworms, Shoults-Wilson et al. (2011) concluded that soil conditions are a more important determinant of AgNP toxicity than size.[52] This is consistent with our finding that model predictions of Ag^+ release are relatively insensitive to the rates of AgNP oxidation and sulfidation (SI Table S4) compared to model variables describing the environmental conditions.

In several environmental risk studies of nanosilver,[19−21] predicted environmental concentrations (PECs) were compared to no observed effect concentrations (NOECs) or LC_{50} values for the pristine Ag^0 NPs. Nanosilver risk is overestimated by this approach, which overlooks the significant reduction in acute toxicity expected after AgNP sulfidation.[3] To improve risk estimates, sediment PECs should be compared to toxicity thresholds for partially and fully sulfidized AgNPs.

Even under oxic conditions, the toxic species Ag^+ represents <0.01 wt-% of the total silver in the system. Thus the toxicity of environmentally transformed AgNPs and released ions may be quite low. However, AgNP risk may be underestimated if, as has historically been the case, Ag^+ is considered the only bioavailable silver species in freshwater environments.[13,29,34] Ingestion, uptake, or surface interactions with unsulfidized or partially sulfidized AgNPs by aquatic plants and sediment organisms may lead to higher exposures.[35]

Because Ag_2S is the principle product of AgNP transformation, the rate of oxidation of sulfur in Ag_2S is of particular interest. Previous work reveals that complexation with metal ions stabilizes thiols and sulfides against oxidation under aerobic conditions.[3] Although Ag_2S is highly stable against dissolution ($K_{sp} = 5.92 \times 10^{-51}$),[3,53] Ag_2S can exhibit greater solubility in the presence of sediments. The authors suggest this occurs because Fe(III) in the sediments facilitates oxidation.[42]

At concentrations orders of magnitude higher than observed here (≥10 mmol Ag/m^3), Ag^+ has been shown to transform into Ag^0 NPs in the presence of reduced humic acids.[54,55] This reaction occurs most rapidly in anoxic and suboxic environments. Because FeS and organic matter act as competing ligands in such environments, we do not anticipate that the in situ formation of Ag^0 NPs will play a significant role in nanoparticle fate for low-level releases of Ag^+ in sediments.

Future experimental work may reveal that other oxidants (e.g., Fe^{3+}, Mn^{4+}, NO_3^-, SO_4^{2-}) can oxidize AgNP in sediments under nonequilibrium conditions. One strength of our approach is the ease with which different oxidants or transformative processes (e.g., bacterially mediated oxidation of sulfur in Ag_2S) can be incorporated into the model.

Regulatory and industry decision-making for the safe production, use, and disposal of nanomaterials requires models that can track the environmentally relevant species. Although process-based models capable of describing the temporal evolution of particle size and aggregation state are highly desirable, they present unique theoretical challenges and computational demands. This work reveals that a mass balance model with no explicit inclusion of aggregation can successfully reproduce observations from a freshwater mesocosm experiment.

By omitting aggregation, the model assumes AgNPs mix in the sediment at approximately the same rate as the sediment particles themselves. Since AgNPs are largely expected to heteroaggregate (and thus cotransport) with sediments in natural environments,[26] this assumption appears justified. However, since the overall particle mixing rate (D_p) was determined by calibration,

there is no way to test the assumption in this work. In general, data collected at high spatial and temporal density are needed on another AgNP type or on a different environmental system to validate the model. Nonetheless, we believe the incorporation of nanoparticle chemistry into a conventional mass balance sediment metal modeling framework represents a significant step toward more accurate environmental risk models for nanoparticles.[56]

■ ASSOCIATED CONTENT

Supporting Information

Supporting Information provides model details, including reaction equations and implementation specifics for an exponentially expanding finite difference grid. SI also includes additional model output for pulse inputs and constant inputs of AgNPs.This material is available free of charge via the Internet at http://pubs.acs.org.

■ AUTHOR INFORMATION

Corresponding Author

*(E.A.S.) Phone: (412)-268-3756; fax: (412) 268-3757; e-mail: casman@andrew.cmu.edu.

Notes

The authors declare no competing financial interest.

■ ACKNOWLEDGMENTS

We are grateful to Professor Mitchell J. Small for suggestions and advice. This work was supported by the NSF NEEP (Nanotechnology, Environmental Effects, and Policy) IGERT fellowship program (0966227) and was based on work supported by the U.S. EPA Science to Achieve Results program (R834574), Transatlantic Initiative for Nanotechnology and the Environment (TINE) and the National Science Foundation (NSF and the Environmental Protection Agency (EPA) under NSF Cooperative Agreement EF-0830093, Center for the Environmental Implications of Nanotechnology (CEINT). Any opinions, findings, conclusions or recommendations expressed in this material are those of the authors and do not necessarily reflect the views of the NSF or the EPA. This work has not been subjected to EPA review and no official endorsement should be inferred. Amy Dale acknowledges the ARCS (Achievement Rewards for College Scientists) Foundation for additional financial support.

■ REFERENCES

(1) *2010 Nanotechnology Research Review*, Report Code: NAN047B; Business Communications Company, 2011; www.bccresearch.com/report/2010-nanotechnology-review-nan047b.html.

(2) Analysis of Consumer Products, Nanotechnology Project, Project on Emerging Nanotechnologies, Woodrow Wilson International Center for Scholars, 2012. www.nanotechproject.org/inventories/consumer/analysis_draft/.

(3) Levard, C.; Hotze, E. M.; Lowry, G. V.; Brown, G. E., Jr Environmental transformations of silver nanoparticles: Impact on stability and toxicity. *Environ. Sci. Technol.* **2012**, *46* (13), 6900−6914.

(4) Keller, A. A.; McFerran, S.; Lazareva, A.; Suh, S. Global life cycle releases of engineered nanomaterials. *J. Nanopart. Res.* **2013**, *15* (6), 1−17.

(5) Benn, T. M.; Westerhoff, P. Nanoparticle silver released into water from commercially available sock fabrics. *Environ. Sci. Technol.* **2008**, *42* (11), 4133−4139.

(6) Kaegi, R.; Voegelin, A.; Sinnet, B.; Zuleeg, S.; Hagendorfer, H.; Burkhardt, M.; Siegrist, H. Behavior of metallic silver nanoparticles in a pilot wastewater treatment plant. *Environ. Sci. Technol.* **2011**, *45* (9), 3902−3908.

(7) Levard, C.; Reinsch, B. C.; Michel, F. M.; Oumahi, C.; Lowry, G. V.; Brown, G. E., Jr Sulfidation processes of PVP-coated silver nanoparticles in aqueous solution: Impact on dissolution rate. *Environ. Sci. Technol.* **2011**, *45* (12), 5260−5266.

(8) Liu, J.; Hurt, R. H. Ion release kinetics and particle persistence in aqueous nano-silver colloids. *Environ. Sci. Technol.* **2010**, *44* (6), 2169−2175.

(9) Liu, J.; Sonshine, D. A.; Shervani, S.; Hurt, R. H. Controlled release of biologically active silver from nanosilver surfaces. *ACS nano* **2010**, *4* (11), 6903.

(10) Dobias, J.; Bernier-Latmani, R. Silver release from silver nanoparticles in natural waters. *Environ. Sci. Technol.* **2013**, *47* (9), 4140−4146.

(11) Ma, R.; Levard, C. m.; Marinakos, S. M.; Cheng, Y.; Liu, J.; Michel, F. M.; Brown, G. E., Jr; Lowry, G. V. Size-controlled dissolution of organic-coated silver nanoparticles. *Environ. Sci. Technol.* **2011**, *46* (2), 752−759.

(12) Fabrega, J.; Luoma, S. N.; Tyler, C. R.; Galloway, T. S.; Lead, J. R. Silver nanoparticles: Behaviour and effects in the aquatic environment. *Environ. Int.* **2011**, *37* (2), 517−531.

(13) Luoma, S. N. *Silver Nanotechnologies and the Environment: Old Problems or New Challenges*?; Project on Emerging Nanotechnologies, Woodrow Wilson International Center for Scholars, 2008.

(14) Liu, J.; Pennell, K. G.; Hurt, R. H. Kinetics and mechanisms of nanosilver oxysulfidation. *Environ. Sci. Technol.* **2011**, *45* (17), 7345−7353.

(15) Kim, B.; Park, C. S.; Murayama, M.; Hochella, M. F. Discovery and characterization of silver sulfide nanoparticles in final sewage sludge products. *Environ. Sci. Technol.* **2010**, *44* (19), 7509.

(16) Reinsch, B.; Levard, C.; Li, Z.; Ma, R.; Wise, A.; Gregory, K.; Brown, G., Jr; Lowry, G. Sulfidation of silver nanoparticles decreases Escherichia coli growth inhibition. *Environ. Sci. Technol.* **2012**, *46* (13), 6992−7000.

(17) Choi, O.; Hu, Z. Nitrification inhibition by silver nanoparticles. *Water Sci. Technol.* **2009**, *59* (9), 1699.

(18) Blaser, S. A.; Scheringer, M.; MacLeod, M.; Hungerbühler, K. Estimation of cumulative aquatic exposure and risk due to silver: Contribution of nano-functionalized plastics and textiles. *Sci. Tot. Environ.* **2008**, *390* (2), 396−409.

(19) Mueller, N. C.; Nowack, B. Exposure modeling of engineered nanoparticles in the environment. *Environ. Sci. Technol.* **2008**, *42* (12), 4447−4453.

(20) Gottschalk, F.; Ort, C.; Scholz, R.; Nowack, B. Engineered nanomaterials in rivers−Exposure scenarios for Switzerland at high spatial and temporal resolution. *Environ. Pollut.* **2011**, *159* (12), 3439−3445.

(21) Gottschalk, F.; Sonderer, T.; Scholz, R. W.; Nowack, B. Modeled environmental concentrations of engineered nanomaterials (TiO_2, ZnO, Ag, CNT, fullerenes) for different regions. *Environ. Sci. Technol.* **2009**, *43* (24), 9216−9222.

(22) Arvidsson, R.; Molander, S.; Sandén, B. A.; Hassellöv, M. Challenges in exposure modeling of nanoparticles in aquatic environments. *Hum. Ecol. Risk Assess.* **2011**, *17* (1), 245−262.

(23) Praetorius, A.; Scheringer, M.; Hungerbühler, K. Development of environmental fate models for engineered nanoparticles: A case study of TiO_2 Nanoparticles in the Rhine River. *Environ. Sci. Technol.* **2012**, *46* (Waterscience and technology12), 6705−6713.

(24) Elimelech, M.; Jia, X.; Gregory, J.; Williams, R. *Particle Deposition and Aggregation: Measurement, Modelling and Simulation*; Butterworth-Heinemann, 1998.

(25) Petosa, A. R.; Jaisi, D. P.; Quevedo, I. R.; Elimelech, M.; Tufenkji, N. Aggregation and deposition of engineered nanomaterials in aquatic environments: Role of physicochemical interactions. *Environ. Sci. Technol.* **2010**, *44* (17), 6532−6549.

(26) Quik, J. T. K.; Stuart, M. C.; Wouterse, M.; Peijnenburg, W.; Hendriks, A. J.; van de Meent, D. Natural colloids are the dominant

factor in the sedimentation of nanoparticles. *Environ. Toxicol. Chem.* **2012**, *31* (), 1019−1022.
(27) Keller, A. A.; Wang, H.; Zhou, D.; Lenihan, H. S.; Cherr, G.; Cardinale, B. J.; Miller, R.; Ji, Z. Stability and aggregation of metal oxide nanoparticles in natural aqueous matrices. *Environ. Sci. Technol.* **2010**, *44* (6), 1962−1967.
(28) Zhou, D.; Abdel-Fattah, A.; Keller, A. A. Clay particles destabilize engineered nanoparticles in aqueous environments. *Environ. Sci. Technol.* **2012**, *46* (14), 7520−7526.
(29) Burton, J., G.A. Sediment quality criteria in use around the world. *Limnology* **2002**, *3* (2), 65−76.
(30) Unrine, J. M.; Shoults-Wilson, W. A.; Zhurbich, O.; Bertsch, P. M.; Tsyusko, O. V. Trophic transfer of au nanoparticles from soil along a simulated terrestrial food chain. *Environ. Sci. Technol.* **2012**, *46* (17), 9753−9760.
(31) Di Toro, D. M.; Mahony, J. D.; Hansen, D. J.; Berry, W. J. A model of the oxidation of iron and cadmium sulfide in sediments. *Environ. Toxicol. Chem.* **1996**, *15* (12), 2168−2186.
(32) Boudreau, B. P. Metals and models: Diagenic modelling in freshwater lacustrine sediments. *J. Paleolimnol.* **1999**, *22* (3), 227−251.
(33) Di Toro, D. M. *Sediment Flux Modeling*. Wiley-Interscience: New York, 2001.
(34) Di Toro, D. M.; McGrath, J. A.; Hansen, D. J.; Berry, W. J.; Paquin, P. R.; Mathew, R.; Wu, K. B.; Santore, R. C. Predicting sediment metal toxicity using a sediment biotic ligand model: Methodology and initial application. *Environ. Toxicol. Chem.* **2009**, *24* (10), 2410−2427.
(35) Lowry, G. V.; Espinasse, B. P.; Badireddy, A. R.; Richardson, C. J.; Reinsch, B. C.; Bryant, L. D.; Bone, A. J.; Deonarine, A.; Chae, S.; Therezien, M. Long-term transformation and fate of manufactured Ag nanoparticles in a simulated large scale freshwater emergent wetland. *Environ. Sci. Technol.* **2012**, *46* (13), 7027−7036.
(36) Kaegi, R.; Voegelin, A.; Ort, C.; Sinnet, B.; Thalmann, B.; Krismer, J.; Hagendorfer, H.; Elumelu, M.; Mueller, E. Fate and transformation of silver nanoparticles in urban wastewater systems. *Water Res.* **2013**, *47* (12), 3866−3877.
(37) Levard, C.; Mitra, S.; Yang, T.; Jew, A.; Badireddy, A. R.; Lowry, G. V.; Brown, G. E. The effect of chloride on the dissolution rate of silver nanoparticles and toxicity to E. coli. *Environ. Sci. Technol.* **2013**, *47* (11), 5738−5745.
(38) Schwarzenbach, R. P.; Gschwend, P. M.; Imboden, D. M. *Environmental Organic Chemistry*; Wiley-Interscience, 2005.
(39) Ramaswami, A.; Milford, J. B.; Small, M. J. *Integrated Environmental Modeling: Pollutant Transport, Fate, And Risk in the Environment*, 1st ed.; John Wiley & Sons: New York, NY, 2005.
(40) Boudreau, B. P. *Diagenetic Models and Their Implementation: Modelling Transport and Reactions in Aquatic Sediments*; Springer: Berlin, 1997.
(41) Boudreau, B. P. Is burial velocity a master parameter for bioturbation? *Geochim. Cosmochim. Acta* **1994**, *58* (4), 1243−1249.
(42) Di Toro, D. M.; Mahony, J. D.; Carbonaro, R. F.; DeMarco, T.; Morrissey, J. C.; Pablo, R. J.; Page, J. J.; Shadi, T. S., *The Oxidation of Silver Sulfide and Other Heavy Metal Sulfides in Sediments*; Andren, A., Bober, T. W., Eds.; Argentum V conference proceedings; University of Wisconsin System, Sea Grant Institute: University of Wisconsin System, Sea Grant Institute, 1998.
(43) Gąsiorowski, M. Deposition rate of lake sediments under different alternative stable states. *Geochronometria* **2008**, *32* (-1), 29−35.
(44) Rose, N. L.; Morley, D.; Appleby, P. G.; Battarbee, R. W.; Alliksaar, T.; Guilizzoni, P.; Jeppesen, E.; Korhola, A.; Punning, J. M. Sediment accumulation rates in European lakes since AD 1850: Trends, reference conditions and exceedence. *J. Paleolimnol.* **2011**, *45* (4), 447−468.
(45) Allison, J. D.; Allison, T. L., Partition coefficients for metals in surface water, soil, and waste. Rep. EPA/600/R-05, 2005, *74*.
(46) Feldberg, S. W. Optimization of explicit finite-difference simulation of electrochemical phenomena utilizing an exponentially expanded space grid: Refinement of the Joslin-Pletcher algorithm. *J. Electroanal. Chem. Interfacial Electrochem.* **1981**, *127* (1), 1−10.
(47) Joslin, T.; Pletcher, D. The digital simulation of electrode processes. procedures for conserving computer time. *J. Electroanal. Chem. Interfacial Electrochem.* **1974**, *49* (2), 171−186.
(48) Neubauer, S. C.; Miller, W. D.; Anderson, I. C. Carbon cycling in a tidal freshwater marsh ecosystem: A carbon gas flux study. *Mar. Ecol.: Prog. Ser.* **2000**, *199*, 13−30.
(49) Sotiriou, G. A.; Meyer, A.; Knijnenburg, J. T.; Panke, S.; Pratsinis, S. E. Quantifying the origin of released Ag+ ions from nanosilver. *Langmuir* **2012**, *28* (45), 15929−15936.
(50) Cowan, J. L.; Boynton, W. R. Sediment-water oxygen and nutrient exchanges along the longitudinal axis of Chesapeake Bay: Seasonal patterns, controlling factors and ecological significance. *Estuaries* **1996**, *19* (3), 562−580.
(51) Kristensen, E. Organic matter diagenesis at the oxic/anoxic interface in coastal marine sediments, with emphasis on the role of burrowing animals. *Hydrobiologia* **2000**, *426* (1), 1−24.
(52) Shoults-Wilson, W. A.; Reinsch, B. C.; Tsyusko, O. V.; Bertsch, P. M.; Lowry, G. V.; Unrine, J. M. Role of particle size and soil type in toxicity of silver nanoparticles to earthworms. *Soil Sci. Soc. Am. J.* **2011**, *75* (2), 365−377.
(53) Lombi, E.; Donner, E.; Taheri, S.; Tavakkoli, E.; Jämting, Å. K.; McClure, S.; Naidu, R.; Miller, B. W.; Scheckel, K. G.; Vasilev, K. Transformation of four silver/silver chloride nanoparticles during anaerobic treatment of wastewater and post-processing of sewage sludge. *Environ. Pollut.* **2013**, *176*, 193−197.
(54) Maurer, F.; Christl, I.; Kretzschmar, R. Reduction and reoxidation of humic acid: Influence on spectroscopic properties and proton binding. *Environ. Sci. Technol.* **2012**, *44* (15), 5787−5792.
(55) Akaighe, N.; MacCuspie, R. I.; Navarro, D. A.; Aga, D. S.; Banerjee, S.; Sohn, M.; Sharma, V. K. Humic acid-induced silver nanoparticle formation under environmentally relevant conditions. *Environ. Sci. Technol.* **2011**, *45* (9), 3895−3901.
(56) Lowry, G. V.; Gregory, K. B.; Apte, S. C.; Lead, J. R. Transformations of nanomaterials in the environment. *Environ. Sci. Technol.* **2012**, *46* (13), 6893−6899.